ORGANIZATION FOR NUCLEAR RESEARCH

A_2^- PRODUCTION IN THE REACTION $\pi^- p \to K^- K_S^0 p$ AT 9.8 AND 18.8 GeV

CERN-Munich (MPI) Collaboration

V. Chabaud, B. Hyams, C. Jones and P. Weilhammer

CERN, Geneva, Switzerland

W. Blum, H. Dietl, G. Grayer[1], W. Kern[2], W. Koch[3], E. Lorenz, G. Lütjens, G. Lutz, J. Meissburger[4] and U. Stierlin

Max-Planck Institut für Physik und Astrophysik, Munich, Germany

ABSTRACT

Results of two spark chamber experiments on A_2^- production in the reaction $\pi^- p \to K^- K_S^0 (\to \pi^+\pi^-) p$ at 9.8 and 18.8 GeV are presented. Decay angular distributions and differential cross-sections are given, and the energy dependence of the cross-section $\sigma[\pi^- p \to A_2^- (\to K^- K^0) p]$ is compared with results from $\pi^- p \to A_2^- (\to 3\pi) p$.

Geneva - 18 July 1978

(Submitted to Nuclear Physics B)

---

1) Now at Rutherford Laboratory, Chilton, Didcot, Oxfordshire, UK.

2) Now at Southeastern Massachusetts University, N. Dartmouth, Mass., USA.

3) Now at DESY, Hamburg, Germany.

4) Now at Institut für Kernphysik, Jülich, Germany.

1. INTRODUCTION

In this paper we report on measurements of A_2^- production in the reaction

$$\pi^- p \to K^- K_S^0 (\to \pi^+ \pi^-) p \quad . \tag{1}$$

This experiment was performed at the CERN Proton Synchrotron (PS) at 9.8 and 18.8 GeV incident momentum. The detector was the CERN-Munich spectrometer[1]. The aim of this experiment was to study the s- and t-dependence on the A_2 production cross-section, and the decay angular distribution of the $K^- K_S^0$ system in the mass region from threshold to 1.6 GeV.

The production of charged A_2 mesons has been studied in many electronic and bubble chamber experiments both near threshold[2-5] and at high energies[6-14]. At high energies it exhibits some interesting properties:

i) the $A_2^\pm$ is produced by natural parity exchange in an almost pure state $\left(|j,m\rangle = |2,1\rangle + |2,-1\rangle \text{ in the t-channel helicity frame}\right)$;

ii) the cross-section decreases rather slowly with increasing energy.

In most previous experiments of $A_2^\pm$ production in pion-proton or pion-nucleon interaction, the $A_2^\pm$ was observed by its decay into a three-pion final state. In order to extract the $A_2^\pm$ meson amplitude $J^P = 2^+$ from the dominant 1^+ and 2^- states, a complex partial wave analysis had to be performed. An alternative possibility for studying $A_2^\pm$ production is to measure a two-body decay of the $A_2^\pm$ such as $K^\pm \bar{K}^0$ (or $\pi^\pm \eta$). In this channel the $A_2^\pm$ is observed with little background from other states, since only states with natural spin-parity can occur. In addition, the two-body decay involves fewer kinematic parameters. The low background and the small number of kinematic variables permit a straightforward spin and helicity determination of the A_2. Using the same apparatus at two different energies reduces systematic errors in the study of the energy dependence of the cross-section. A difficulty of the study of the channel $A_2^\pm \to K^\pm K_S^0$ is the small branching ratio of less than 10%.

2. APPARATUS

The experimental set-up is shown in Fig. 1 and is described in detail in Ref. 1.

The experiment used an unseparated pion beam from the PS. The incident beam was defined by four scintillation counters S_1, ..., S_4. Pions were tagged with two threshold Čerenkov counters $\check{C}_1$ and $\check{C}_2$. Incident pions interacted in a 50 cm liquid-hydrogen target H_2. The directions of the beam particle and the charged forward-going secondaries were measured in three sets of wire spark chambers, W_1, W_2, and W_3, with magnetostrictive read-out. A wide-gap magnet of 2 T·m bending power served, together with the chamber sets W_2 and W_3, as a momentum analyser for the forward-going secondary particles.

Except for a beam entrance hole and an exit window, the target was completely surrounded by lead scintillation sandwich counters S_5 in order to reject events with emission of π^0's or more than one charged recoil particle. The anticoincidence counters S_7, forming a window in front of the analysing magnet, and S_8, lining all magnet gap faces, further suppressed unwanted triggers. The scintillation counter S_6, with a small hole on the beam trajectory, sensed interactions with forward-going charged particles. The 32-element hodoscope S_9 served for the selection of three charged secondary tracks. A small counter S_{10} vetoed beam particles that interacted at the end of the apparatus.

The complete trigger condition was:

$$\left[S_1 \cdot S_2 \cdot S_3 \cdot \overline{S_4}\right] \cdot S_6 \cdot \overline{S_{10}} \cdot \overline{S_5(\geq 2 \text{ hits})} \cdot \overline{S_7} \cdot \overline{S_8} \cdot S_9(= 3 \text{ hits}) \ .$$

3. DATA PROCESSING AND EVENT SELECTION

A total of 0.8×10^6 triggers at 9.8 GeV and 1.3×10^6 triggers at 18.8 GeV were recorded in this experiment. Only a small fraction of these had the two-vertex topology of reaction (1). In order to separate them from the much more numerous triggers from the reaction $\pi^- p \to \pi^- \pi^+ \pi^- p$, various cuts were applied

during an early stage of the event reconstruction: i) three tracks were required in the spark chamber set W_2, thus limiting the V^0 decay volume between the primary vertex and the beginning of W_2; ii) from the beam trajectory and the three secondary trajectories, the point of the closest approach was calculated. In the case of a genuine single-vertex solution, the event was rejected. Furthermore, two secondary tracks had to form a vertex separated from the intercept of the remaining track with the beam trajectory. Only those events where the V^0 vertex was downstream from the production vertex were fully reconstructed.

Figure 2 shows the invariant $\pi^+\pi^-$ mass of the V^0's at 18.8 GeV with a clear K^0 signal. Furthermore, we selected only events with a V^0 mass between 486 and 509 MeV. Figures 3a and 3b show the square of the mass of the invisible recoil particle after K^-K^0 assignment to the forward-going system. A peak around the proton mass is observed at both data sets. The width of the distributions is compatible with the expected resolution for a missing proton. For the final event selection, we required the square of the missing mass (MM^2) to be between 0.5 and 1.25 GeV^2 at 9.8 GeV, and between 0.15 and 1.4 GeV^2 at 18.8 GeV. The final samples (Figs. 4a and 4b) contain 995 events at 9.8 GeV and 2150 events at 18.8 GeV. Small background contributions to these samples come from the following reactions:

$$\pi^- p \to K^- K^0 (p\pi^0)$$

$$\to K^- K^0 (n\pi^+)$$

$$\to \pi^- K^0 \Sigma^+ \quad .$$

From the MM^2 distribution, we estimate a background in our samples of 3.8 ± 0.5% at 9.8 GeV and 5.2 ± 1.0% at 18.8 GeV.

4. ACCEPTANCE CORRECTION AND ABSOLUTE CROSS-SECTION DETERMINATION

In order to obtain the differential cross-sections $d\sigma/dM$, $d\sigma/dt$, and $d\sigma/d\Omega$, and the absolute cross-section, the observed data have to be corrected for losses caused by our detector.

For fixed s and an unpolarized target, reaction (1) can be described by four kinematic variables:

$m_{K\bar{K}}$ = the invariant K^-K^0 mass

t = the square of the four-momentum transfer from the initial to the final proton

θ,ϕ = the decay angles of the K^- in the t-channel helicity frame of the K^-K^0 system.

The losses caused by our detector can be subdivided into a class which depends on the event configuration, i.e. on the kinematic variables, and a class which is independent of the event configuration.

The configuration-dependent losses from secondary interactions and decay in flight of the K^- and the $\pi^\pm$ were corrected by weighting individual events. The mean value and the range of these weight factors was

$$\langle W(9.8\ \text{GeV})\rangle = 1.35\ ; \quad \text{varying between 1.20 and 1.70}\ ;$$

$$\langle W(18.8\ \text{GeV})\rangle = 1.25\ ; \quad \text{varying between 1.09 and 1.40}\ .$$

The most important configuration-dependent loss was caused by the geometry of our spectrometer, covering only about 0.15 sr. Figure 5 shows examples of the acceptance $A(m_{K\bar{K}})$ for an isotropically decaying K^-K^0 system at two t-values. For the acceptance correction the same procedure as in Ref. 1 was applied. The data were binned in $m_{K\bar{K}}$ and t. For fixed $m_{K\bar{K}}$ and t, the produced decay angular distribution $I_{prod}(\Omega)$ can be written in terms of spherical harmonics $Y_L^M(\Omega)$:

$$I_{prod}(\Omega) = N_{prod} \sum_{L=0}^{L_{max}} \sum_{M=0}^{L} \varepsilon_M \left\langle Y_L^M \right\rangle \cdot Y_L^M(\Omega)$$

with N_{prod} = produced number of events in $m_{K\bar{K}}$, t-bin, $\varepsilon_M = 1$ for $M = 0$ and $\varepsilon_M = 2$ for $M \geq 1$ $\left[\left\langle Y_L^M \right\rangle, Y_L^M(\Omega)\right.$ is shorthand for $\left.\left\langle \text{Re}\ Y_L^M \right\rangle, \text{Re}\ Y_L^M(\Omega)\right]$.

The $\langle Y_L^M \rangle$ are the normalized spherical harmonic moments. The observed angular distribution $I_{obs}(\Omega)$ is connected to the moments by

$$I_{obs}(\Omega) = A(\Omega) \cdot N_{prod} \sum_{L=0}^{L_{max}} \sum_{M=0}^{L} \varepsilon_M \langle Y_L^M \rangle Y_L^M(\Omega) \quad ,$$

with $A(\Omega)$ being the acceptance for events with the decay angles θ and ϕ; $A(\Omega)$ was calculated by the Monte Carlo method. The moments were determined by maximum likelihood fits. Owing to the small number of events, L_{max} was limited to 4 (S-, P-, and D-waves) below 1.4 GeV. Between 1.4 and 1.6 GeV mass, also $\langle Y_5^0 \rangle$, $\langle Y_5^1 \rangle$, $\langle Y_6^0 \rangle$, and $\langle Y_6^1 \rangle$ were added to allow for an F-wave (g meson). Most of the moments were found to be compatible with zero and were successively eliminated from the fits. This reduced the number of free parameters and permitted a fine mass binning in subsequent fits. Finally, only the four moments $\langle Y_2^0 \rangle$, $\langle Y_2^2 \rangle$, $\langle Y_4^0 \rangle$, and $\langle Y_4^2 \rangle$ were found to be significant below 1.6 GeV mass. The final fits yielded these four moments and the true number of produced events N_{prod}, together with their statistical errors.

For the absolute cross-section determination for the number of incident pions, the configuration-independent losses were taken into account by a global multiplication factor F. This factor accounted for a series of small corrections listed in Table 1.

The following total cross-sections from 1.0 to 1.6 GeV in mass and from t_{min} to -0.4 GeV^2 in t were determined:

$$\sigma[\pi^- p \to K^- K_S^0 (\to \pi^+ \pi^-) p] = 2.93 \pm 0.27 \ \mu b \text{ at } 9.8 \text{ GeV} \ ,$$

$$\sigma[\pi^- p \to K^- K_S^0 (\to \pi^+ \pi^-) p] = 1.61 \pm 0.14 \ \mu b \text{ at } 18.8 \text{ GeV} \ .$$

The 'one-event' cross-sections are

$$\sigma(1 \text{ event}) = 0.171 \pm 0.015 \text{ nb} \quad \text{at } 9.8 \text{ GeV} \ ,$$

$$\sigma(1 \text{ event}) = 0.205 \pm 0.016 \text{ nb} \quad \text{at } 18.8 \text{ GeV} \ .$$

5. THE DIFFERENTIAL CROSS-SECTIONS $d\sigma/dM$, $d\sigma/dt$ AND THE MOMENTS $\langle Y_\ell^m \rangle$ AS A FUNCTION OF MASS

Figure 6 shows the corrected mass spectra for $|t| \leq 0.4$ GeV^2. In both distributions only the signal of the A_2 around 1300 MeV is observed. Contrary to the observations in the reaction $\pi^- p \to K^+K^- n$ at the same energies[15] no threshold enhancement is seen.

Figure 7 (Table 2) shows the differential cross-sections $d\sigma/dt$ integrated over the mass range 1.20-1.42 GeV. Also displayed is the differential cross-section of $d\sigma/dt$ from the reaction $\pi^- p \to K^+K^- n$ at 18.4 GeV [15], where isospin I = 0 partial waves are also present. A remarkable difference is observed.

Figure 8 (Tables 3a and 3b) shows the four moments $\langle Y_2^0 \rangle$, $\langle Y_2^2 \rangle$, $\langle Y_4^0 \rangle$, and $\langle Y_4^2 \rangle$ as a function of $m_{K\bar{K}}$, after integration in t, from t_{min} to -0.4 GeV^2. As already mentioned, the other moments were consistent with zero.

6. DETERMINATION OF THE A_2 RESONANCE PARAMETERS

To determine the resonance parameters of the A_2, we parametrized the mass spectrum by a spin-2 Breit-Wigner distribution and a background distribution:

$$d\sigma/dm = C \left[\frac{m \cdot m_0 \cdot \Gamma}{(m^2 - m_0^2)^2 + m^2\Gamma^2} + BG \right] , \qquad (5)$$

with

$$\Gamma = \Gamma_0 \left(\frac{q}{q_0}\right)^5 \frac{R^4 q_0^4 + 3R^2 q_0^2 + q}{R^4 q^4 + 3R^2 q^2 + q}$$

m = mass of the $K^- K_S^0$ system

m_0, Γ_0 = mass, width of the A_2 resonance

q = c.m. momentum of the K^- in the $K^- K^0$ system

q_0 = q at A_2 resonance

R = range parameter = 1 fermi

C = normalization constant.

The background (BG) was either constant or varying linearly with mass

$$BG = C_1 \; ; \quad \text{or} \quad BG = C_1 + C_2 \cdot m \; .$$

The fit used a χ^2 minimization in the mass range from 1.0 to 1.6 GeV and $|t| < 0.4$ GeV^2. The mass resolution of the spectrometer of $\sigma = 5.7$ MeV at 1300 MeV was folded in.

The results of the fits are given in Table 4. The fitted shape of the spectrum and the background contribution are indicated in Fig. 6. As is evident from the figure, the A_2 is sufficiently parametrized by a single pole resonance.

7. THE SPIN DENSITY MATRIX ELEMENTS IN THE A_2 REGION

From the four fitted moments $\langle Y_\ell^m \rangle$, we calculated the density matrix elements ρ_{ik}^{22} in the A_2 region ($1.20 < m_{K^-K^0} < 1.42$ GeV) for several t-intervals:

$$\begin{aligned} \rho_{00} &= 1.585 \langle Y_2^0 \rangle + 2.127 \langle Y_4^0 \rangle + 0.2 \; , \\ \rho_{11} &= 0.793 \langle Y_2^0 \rangle - 1.418 \langle Y_4^0 \rangle + 0.2 \; , \\ \rho_{1-1} &= -1.942 \langle Y_2^2 \rangle - 2.242 \langle Y_4^2 \rangle \; , \\ \text{Re } \rho_{20} &= -1.585 \langle Y_2^2 \rangle + 1.372 \langle Y_4^2 \rangle \; . \end{aligned} \tag{6}$$

The results are listed in Tables 5a and 5b and shown in Fig. 9 as a function of t. Except for very small values of t, ρ_{11} and ρ_{1-1} are found to be near their maximum possible values, whereas ρ_{00} and Re ρ_{20} are decreasing to small values with increasing $|t|$. We attribute this behaviour to an increase of A_2 production by natural parity exchange relative to the background and to the production by unnatural parity exchange. The available statistics, and the method of acceptance correction and determination of the moments, excludes a more detailed analysis.

Figures 9a and 9b also display the t-dependence of the combination $\rho^+ = \rho_{11} + \rho_{1-1}$ and $\rho^- = \rho_{11} - \rho_{1-1}$. The combination $\rho_{11} + \rho_{1-1}$ represents the natural parity-exchange part of the A_2 production cross-section. It is fairly

constant for $|t| > 0.1$ GeV^2 at both energies. At 18.8 GeV it approaches 1.0, signifying complete dominance of natural parity exchange and no change in the production mechanism of the A_2 up to a $|t|$ of 0.8 GeV^2. At 9.8 GeV the value of $\rho_{11} + \rho_{1-1}$ is around 0.85.

In order to extract the A_2 production cross-section due to natural parity exchange (NPE), we fitted the following expression to the differential cross-section:

$$\frac{d\sigma^{NPE}}{dt'} = C \cdot B^2 \cdot t' \cdot e^{-Bt'} \quad , \tag{7}$$

with $t' = |t - t_{min}|$

$$C = \sigma^{NPE} = \int_0^\infty \frac{d\sigma^{NPE}}{dt'}\, dt' \quad \text{and} \quad \frac{d\sigma^{NPE}}{dt'} = \rho^+(t') \cdot \frac{d\sigma}{dt'} \quad .$$

Figure 10 shows the differential cross-sections $d\sigma^{NPE}/dt$, and Table 6 lists the results of the fits. The slope parameter B is, within the errors, the same at both energies. The pronounced forward dip accounted for by the factor t' is to be expected for a net helicity-flip-one amplitude. Fits using t'^2 instead of t' were also tried, but they yielded unacceptably low χ^2 probabilities.

8. s-DEPENDENCE OF THE CROSS-SECTION

Expressing the energy dependence of the production cross-section as a power law of the laboratory momentum,

$$\sigma \sim p_{lab}^{-n} \quad , \tag{8}$$

we obtain the following values for n from our restricted cross-sections at the two energies:

n = 1.02 ± 0.17 (from the Breit-Wigner fits a and c, Table 4)

n = 0.89 ± 0.18 (from natural parity exchange, Table 6) .

Figure 11 shows a compilation of the cross-section for A_2^- production by natural parity exchange in the $\pi^+\pi^-\pi^-$ and K^-K^0 decay modes. Fitting the cross-sections of the two channels separately (dashed lines) yielded the two values of the exponent $n(A_2^- \to K\bar{K}) = 0.84 \pm 0.10$ and $n(A_2^- \to \rho\pi) = 0.52 \pm 0.06$. Despite the different momentum range and the different experimental procedures, a combined fit (solid lines) gives an exponent $n = 0.60 \pm 0.06$ with a χ^2 probability of 36%. The fit also determines the branching ratio $R(A_2 \to K\bar{K}/A_2 \to \rho\pi) = 7.75 \pm 1.7\%$. This value is in good agreement with the Particle Data Table world average of $6.7 \pm 0.8\%$.

9. CONCLUSION

We have measured the production of the A_2^- meson in the reaction $\pi^- p \to K^- K_S^0 (\to \pi^+\pi^-) p$ at 9.8 GeV and 18.8 GeV incident momentum. The A_2^- is observed, at both energies, above a small background of other states ($\sim$ 10%) and can be well parametrized with a D-wave Breit-Wigner form. The A_2^- is dominantly produced by natural parity exchange ($\rho_{11} + \rho_{1-1} \approx 1$). The differential cross-section $d\sigma^{NPE}/dt'$ has a dip in the forward direction and is well parametrized by the form $C \cdot t' \cdot e^{Bt'}$. The factor t' is to be expected for a helicity-flip-one amplitude.

The energy dependence of the natural parity-exchange part of the cross-section is parametrized by $\sigma^{NPE} \sim p_{lab}^{-n}$. This experiment yields $n = 0.89 \pm 0.18$ compared to the value $n = 0.51 \pm 0.05$ found by Antipov et al.[6] from a study of A_2 production in the $\rho\pi$ decay mode. However, a common fit to all data, $(\rho\pi)^-$ and $K^-K_S^0$ decay modes, gives $n = 0.64 \pm 0.06$ with an acceptable $\chi^2 = 36\%$, and at the same time a branching ratio $R(A_2 \to K\bar{K}/A_2 \to \rho\pi) = 7.75 \pm 1.7\%$, in good agreement with the Particle Data Table value. Whereas our experiment alone is compatible with an energy dependence of σ^{NPE} expected from the exchange of a ρ or f Regge trajectory ($n = 1$), a fit of all available data yields a cross-section dependence on energy ($n = 0.64 \pm 0.06$) about half way between the weak energy dependence for diffractive-like production and the stronger energy dependence for ρ or f exchange.

REFERENCES

1) G. Grayer et al., Nuclear Phys. B75 (1974) 189.

2) G. Ascoli et al., Phys. Rev. Letters 25 (1970) 962.

3) T.F. Johnston et al., Nuclear Phys. B24 (1970) 253.

4) G. Grayer et al., Phys. Letters 34B (1971) 333.

5) K. Foley et al., Phys. Rev. D 6 (1972) 747.

6) Y.M. Antipov et al., Nuclear Phys. B63 (1973) 175.

7) U. Kruse et al., Phys. Rev. Letters 32 (1974) 23.

8) G. Otter et al., Nuclear Phys. B80 (1974) 1.

9) C.M. Ankenbrandt et al., Phys. Rev. D 8 (1973) 2785.

10) D.J. Crennell et al., Phys. Letters 35B (1971) 185.

11) H.A. Gordon et al., Phys. Rev. Letters 33 (1974) 603.

12) V. Chaloupka et al., Phys. Letters 44B (1973) 211.

13) M.J. Losty et al., Phys. Letters 56B (1975) 96.

14) M. Margolies et al., Phys. Rev. D 14 (1976) 667.

15) G. Hentschel, thesis, University of Munich, 1976;
W. Blum et al., Phys. Letters 57B (1975) 403;
G. Grayer et al., AIP Conference Proceedings 13, p. 117.

Table 1

Geometry-independent correction factors F_i for the cross-section determination

Origin of correction	p_{lab} = 9.8 GeV $F_i \pm \Delta F_i$	p_{lab} = 18.8 GeV $F_i \pm \Delta F_i$
Beam contamination e, μ	1.035 ± 0.010	1.030 ± 0.010
" " K^-, $\bar{p}$	1.020 ± 0.010	1.005 ± 0.000 a)
Beam attenuation in H_2	1.025 ± 0.000 a)	1.025 ± 0.000 a)
Interaction in mylar around H_2	0.990 ± 0.000 a)	0.990 ± 0.000 a)
Interactions in S_2, S_3	1.005 ± 0.000 a)	1.005 ± 0.000 a)
" of secondaries in the set-up	1.085 ± 0.010	1.085 ± 0.010
Anticounter jamming	1.040 ± 0.005	1.020 ± 0.010
Effects in S_9 (array):		
dead space	1.025 ± 0.000 a)	1.025 ± 0.000 a)
δ-ray in fourth counter	1.030 ± 0.005	1.030 ± 0.005
interaction behind array	1.005 ± 0.000 a)	1.005 ± 0.000 a)
δ-ray in S_5	1.005 ± 0.005	1.005 ± 0.005
Electronics + counter inefficiencies	1.010 ± 0.010	1.010 ± 0.010
Electronics dead-time	1.020 ± 0.010	1.000 ± 0.000 a)
Reconstruction losses:		
program inefficiency	1.050 ± 0.030	1.050 ± 0.030
random 4th track	1.020 ± 0.005	1.000 ± 0.005
K^0 mass cut	1.010 ± 0.000 a)	1.015 ± 0.000 a)
Background after K^0 mass cut b)	0.995 ± 0.000 a)	0.995 ± 0.000 a)
Missing-mass cut	1.025 ± 0.005	1.045 ± 0.010
Background after MM cut	0.975 ± 0.005	0.960 ± 0.010
Total correction factor $F = \prod F_i$	1.440 ± 0.110 c)	1.350 ± 0.100 c)

a) Error smaller than 0.25%.

b) After application of all other cuts, i.e. not identical with background of Fig. 2.

c) The over-all error includes the estimate of systematic errors.

Table 2

$d\sigma/dt$ for $1.20 \leq m_{K\bar{K}} \leq 1.42$ GeV

$\Delta\|t\|$ (GeV^2)	$d\sigma/dt$ at 9.8 GeV ($\mu b/GeV^2$)	$d\sigma/dt$ at 18.8 GeV ($\mu b/GeV^2$)
t_{min} - 0.045	4.64 ± 0.68	2.24 ± 0.29
0.045 - 0.08	6.81 ± 0.97	3.08 ± 0.38
0.08 - 0.12	7.16 ± 1.00	3.99 ± 0.44
0.12 - 0.17	7.08 ± 0.95	3.55 ± 0.38
0.17 - 0.22	5.69 ± 0.85	3.13 ± 0.35
0.22 - 0.30	4.95 ± 0.71	3.03 ± 0.31
0.30 - 0.50	2.74 ± 0.39	1.26 ± 0.13
0.50 - 0.80		0.34 ± 0.05

Table 3a

$\langle Y_\ell^m \rangle$ versus $m_{K\bar{K}}$ for $|t| \leq 0.4$ GeV^2 at 9.8 GeV

$m_{K\bar{K}}$ (GeV)	$\langle Y_2^0 \rangle$	$\langle Y_2^2 \rangle$	$\langle Y_4^0 \rangle$	$\langle Y_4^2 \rangle$
1.06 (1.00-1.10)	0.078 ± 0.046	0.006 ± 0.026	0.012 ± 0.043	-0.014 ± 0.030
1.16 (1.10-1.20)	0.662 ± 0.030	-0.042 ± 0.020	-0.045 ± 0.030	-0.031 ± 0.023
1.26 (1.20-1.30)	0.112 ± 0.015	-0.073 ± 0.010	-0.122 ± 0.016	-0.080 ± 0.013
1.34 (1.30-1.40)	0.122 ± 0.015	-0.082 ± 0.007	-0.098 ± 0.017	-0.095 ± 0.009
1.45 (1.40-1.50)	0.060 ± 0.036	-0.072 ± 0.018	-0.064 ± 0.034	-0.040 ± 0.026
1.55 (1.50-1.60)	0.106 ± 0.038	-0.035 ± 0.032	-0.107 ± 0.046	-0.009 ± 0.038

Table 3b

$\langle Y_\ell^m \rangle$ versus $m_{K\bar{K}}$ for $|t| \leq 0.4$ GeV^2 at 18.8 GeV

$m_{K\bar{K}}$ (GeV)	$\langle Y_2^0 \rangle$	$\langle Y_2^2 \rangle$	$\langle Y_4^0 \rangle$	$\langle Y_4^2 \rangle$
1.05 (1.00-1.10)	0.049 ± 0.048	0.011 ± 0.038	-0.062 ± 0.057	0.064 ± 0.068
1.16 (1.10-1.20)	0.062 ± 0.038	-0.047 ± 0.020	-0.034 ± 0.041	-0.041 ± 0.023
1.23 (1.20-1.25)	0.110 ± 0.029	-0.095 ± 0.016	-0.066 ± 0.031	-0.125 ± 0.018
1.28 (1.25-1.30)	0.076 ± 0.014	-0.097 ± 0.009	-0.155 ± 0.014	-0.117 ± 0.011
1.32 (1.30-1.35)	0.107 ± 0.016	-0.093 ± 0.009	-0.125 ± 0.018	-0.105 ± 0.011
1.37 (1.35-1.40)	0.093 ± 0.016	-0.092 ± 0.011	-0.144 ± 0.015	-0.100 ± 0.016
1.42 (1.40-1.45)	0.076 ± 0.024	-0.101 ± 0.018	-0.159 ± 0.028	-0.102 ± 0.025
1.47 (1.45-1.50)	0.051 ± 0.029	-0.098 ± 0.014	-0.131 ± 0.030	-0.095 ± 0.024
1.55 (1.50-1.60)	0.068 ± 0.025	-0.073 ± 0.015	-0.110 ± 0.024	-0.104 ± 0.019

Table 4

Results of fits of A_2 parameters for $1.20 \leq m_{K\bar{K}} \leq 1.42$ GeV

Fit	p_{lab} (GeV)	$m(A_2)$ (GeV)	$\Gamma(A_2)$ (GeV)	Norm. const. C (μb)	Background terms		Prob. (χ^2) (%)	$\sigma(A_2)$ a) (μb)	$\sigma(BG)$ a) (μb)	$\frac{\sigma_{(BG)}}{\sigma_{tot}}$ a) (%)
					C_1 (GeV^{-1})	C_2 (GeV^{-2})				
A	9.8	1.312 ± 0.004	126 ± 11	18.3	0.77 ± 0.11	-	36	1.88 ± 0.11	0.31 ± 0.04	14
B	9.8	1.312 ± 0.004	126 ± 14	18.1	0.69 ± 0.66	0.08 ± 0.66	33	1.87 ± 0.56	0.32 ± 0.55	15
C	18.8	1.318 ± 0.002	113 ± 8	9.6	0.62 ± 0.10	-	29	1.03 ± 0.04	0.13 ± 0.02	11
D	18.8	1.316 ± 0.002	101 ± 8	8.7	-0.40 ± 0.50	0.98 ± 0.48	41	0.97 ± 0.19	0.17 ± 0.19	15

a) Since the parameters in the fit with linear background (B and D) are highly correlated, the error on the background is rather big. This obviously increases the error on the A_2 cross-section $\sigma(A_2)$.

Table 5a

Spin density matrix elements in t-channel helicity frame

ρ^{22}_{ik} versus $|t|$ (GeV^2) for $1.20 \leq m_{K\bar{K}} \leq 1.42$ GeV at 9.8 GeV

$\lvert\bar{t}\rvert$ (GeV^2)	ρ_{00}	ρ_{11}	ρ_{1-1}	Re ρ_{20}	$\rho^+ = \rho_{11} + \rho_{1-1}$	$\rho^- = \rho_{11} - \rho_{1-1}$
0.029 (t_{min} -0.045)	0.323 ± 0.113	0.357 ± 0.070	0.104 ± 0.097	0.084 ± 0.067	0.461 ± 0.120	0.253 ± 0.120
0.064 (0.045-0.08)	0.179 ± 0.071	0.451 ± 0.045	0.366 ± 0.050	0.021 ± 0.033	0.817 ± 0.067	0.085 ± 0.067
0.099 (0.08 -0.12)	0.144 ± 0.072	0.459 ± 0.045	0.352 ± 0.052	-0.035 ± 0.036	0.811 ± 0.069	0.085 ± 0.069
0.146 (0.12 -0.17)	0.249 ± 0.078	0.442 ± 0.049	0.364 ± 0.050	-0.009 ± 0.034	0.806 ± 0.070	0.078 ± 0.070
0.193 (0.17 -0.22)	0.143 ± 0.072	0.433 ± 0.045	0.312 ± 0.059	0.041 ± 0.039	0.745 ± 0.074	0.121 ± 0.074
0.258 (0.22 -0.30)	0.119 ± 0.074	0.446 ± 0.046	0.363 ± 0.051	0.019 ± 0.035	0.809 ± 0.069	0.083 ± 0.069
0.381 (0.30 -0.50)	0.030 ± 0.075	0.493 ± 0.047	0.435 ± 0.053	-0.029 ± 0.036	0.928 ± 0.071	0.058 ± 0.071

Table 5b

Spin density matrix elements in t-channel helicity frame

ρ^{22}_{ik} versus $|t|$ (GeV^2) for $1.20 \leq m_{\overline{KK}} \leq 1.42$ GeV at 18.8 GeV

$\|\bar{t}\|$ (GeV^2)	ρ_{00}	ρ_{11}	ρ_{1-1}	Re ρ_{20}	$\rho^+ = \rho_{11} + \rho_{1-1}$	$\rho^- = \rho_{11} - \rho_{1-1}$
0.029 (t_{min} -0.045)	0.206 ± 0.113	0.412 ± 0.070	0.203 ± 0.063	0.021 ± 0.044	0.615 ± 0.094	0.209 ± 0.094
0.063 (0.045-0.08)	0.105 ± 0.080	0.405 ± 0.049	0.377 ± 0.062	0.002 ± 0.043	0.782 ± 0.079	0.028 ± 0.079
0.101 (0.08 -0.12)	0.013 ± 0.062	0.468 ± 0.039	0.449 ± 0.035	-0.013 ± 0.024	0.917 ± 0.052	0.019 ± 0.052
0.145 (0.12 -0.17)	-0.008 ± 0.040	0.466 ± 0.025	0.480 ± 0.033	-0.047 ± 0.022	0.941 ± 0.041	-0.014 ± 0.041
0.195 (0.17 -0.22)	0.010 ± 0.049	0.473 ± 0.030	0.472 ± 0.029	0.008 ± 0.020	0.945 ± 0.042	0.001 ± 0.042
0.261 (0.22 -0.30)	0.083 ± 0.042	0.472 ± 0.026	0.439 ± 0.031	-0.024 ± 0.021	0.911 ± 0.040	0.033 ± 0.040
0.373 (0.30 -0.50)	0.051 ± 0.048	0.478 ± 0.030	0.527 ± 0.036	-0.011 ± 0.025	1.005 ± 0.047	-0.049 ± 0.047
0.603 (0.50 -0.80)	0.068 ± 0.067	0.460 ± 0.041	0.502 ± 0.055	0.007 ± 0.038	0.962 ± 0.069	-0.042 ± 0.069

Table 6

Results of fits to the differential cross-section $d\sigma^{NPE}/dt$ for natural parity exchange in the A_2 region

	9.8 GeV	18.8 GeV
$\sigma^{NPE}\left[A_2^- \to K^-K_S^0 \to (\pi^+\pi^-)\right]$ for $1.20 \leq m_{K\bar{K}} \leq 1.42$ GeV and all t	1.96 ± 0.16 μb	1.14 ± 0.05 μb
Slope parameter B (GeV^{-2})	7.7 ± 0.6	8.0 ± 0.3
χ^2 probability	60%	52%

Figure captions

Fig. 1 : Schematic layout of the spectrometer

$\check{C}1, \check{C}2$	beam Čerenkov counters
$S_1 \ldots S_{10}$	scintillation counters
$W_1 \ldots W_3$	sets of wire spark chambers
H_2	liquid-hydrogen target
M	spectrometer magnet

Fig. 2 : Invariant $\pi^+\pi^-$ mass distribution for V^0's, p_{lab} = 18.8 GeV.

Fig. 3 : a,b) Missing mass squared distributions for K^-K^0 events at 9.8 and 18.8 GeV. The cuts for a missing proton are indicated by arrows.

Fig. 4 : a,b) observed $K^-K^0_S$ mass spectra at p_{lab} = 9.8 and 18.8 GeV.

Fig. 5 : Acceptance of the spectrometer for Monte Carlo generated events of reaction (1) with isotropic decay of the $K^-K^0_S$ system.

Fig. 6 : a,b) Corrected mass spectra at 9.8 and 18.8 GeV for $|t| < 0.4$ GeV^2.

Fig. 7 : Differential cross-section $d\sigma/dt$ at p_{lab} = 9.8 and 18.8 GeV; $1.20 < m_{K\bar{K}} < 1.42$ GeV.

Fig. 8 : t-channel moments $\langle Y^0_2 \rangle$, $\langle Y^2_2 \rangle$, $\langle Y^0_4 \rangle$, and $\langle Y^2_4 \rangle$ as a function of mass for p_{lab} = 9.8 and 18.8 GeV; $|t| < 0.4$ GeV^2.

Fig. 9 : a,b) t-channel density matrix elements ρ_{00}, ρ_{11}, ρ_{1-1}, Re ρ_{20}, and the combinations $\rho^+ = \rho_{11} + \rho_{1-1}$ and $\rho^- = \rho_{11} - \rho_{1-1}$ as a function of t in the A_2 region (1.20-1.42 GeV).

Fig. 10 : Differential cross-section $d\sigma^{NPE}/dt$ for natural parity exchange in the A_2 region (1.20-1.42 GeV).

Fig. 11 : A compilation of the A_2^- cross-section (σ^{NPE}) as a function of p_{lab} for the $K\bar{K}$ and $\rho\pi$ decay modes:

upper points: $A_2^- \to \rho_0\pi^-$ from Refs. 12 and 6;

lower points: $A_2^- \to K^-K^0$ corrected for all K^0 decay modes;

3.9 GeV data point from Ref. 12;

9.8 and 18.8 GeV data points from this experiment (corrected for $1.2 \leq m_{K\bar{K}} \leq 1.4$ GeV and $|t| \leq 0.8$ GeV^2);

22.4 and 23.9 GeV data points from Ref. 14.

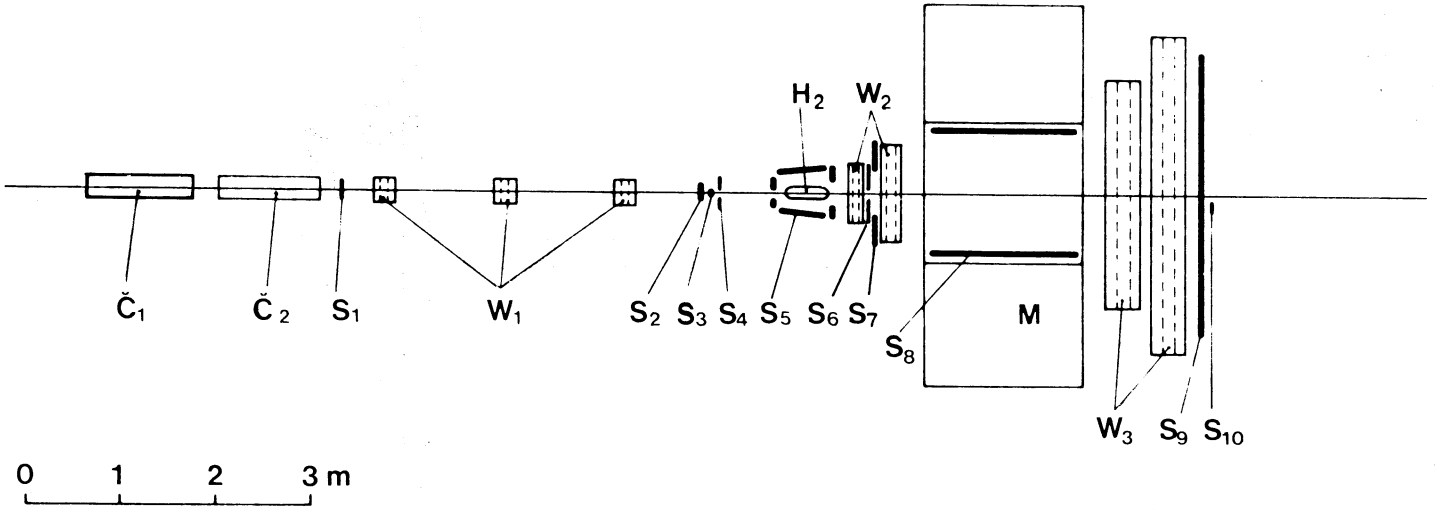

Fig. 1

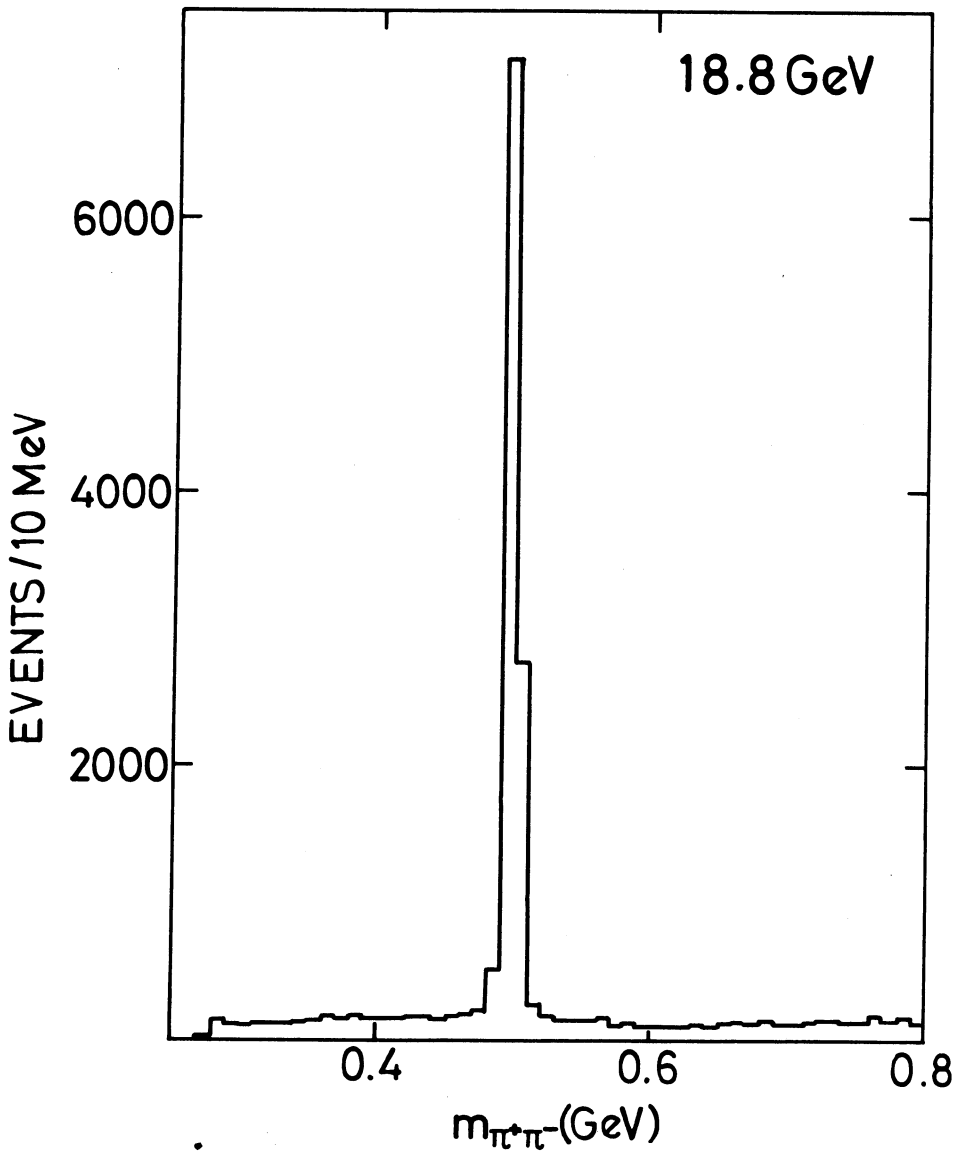

Fig. 2

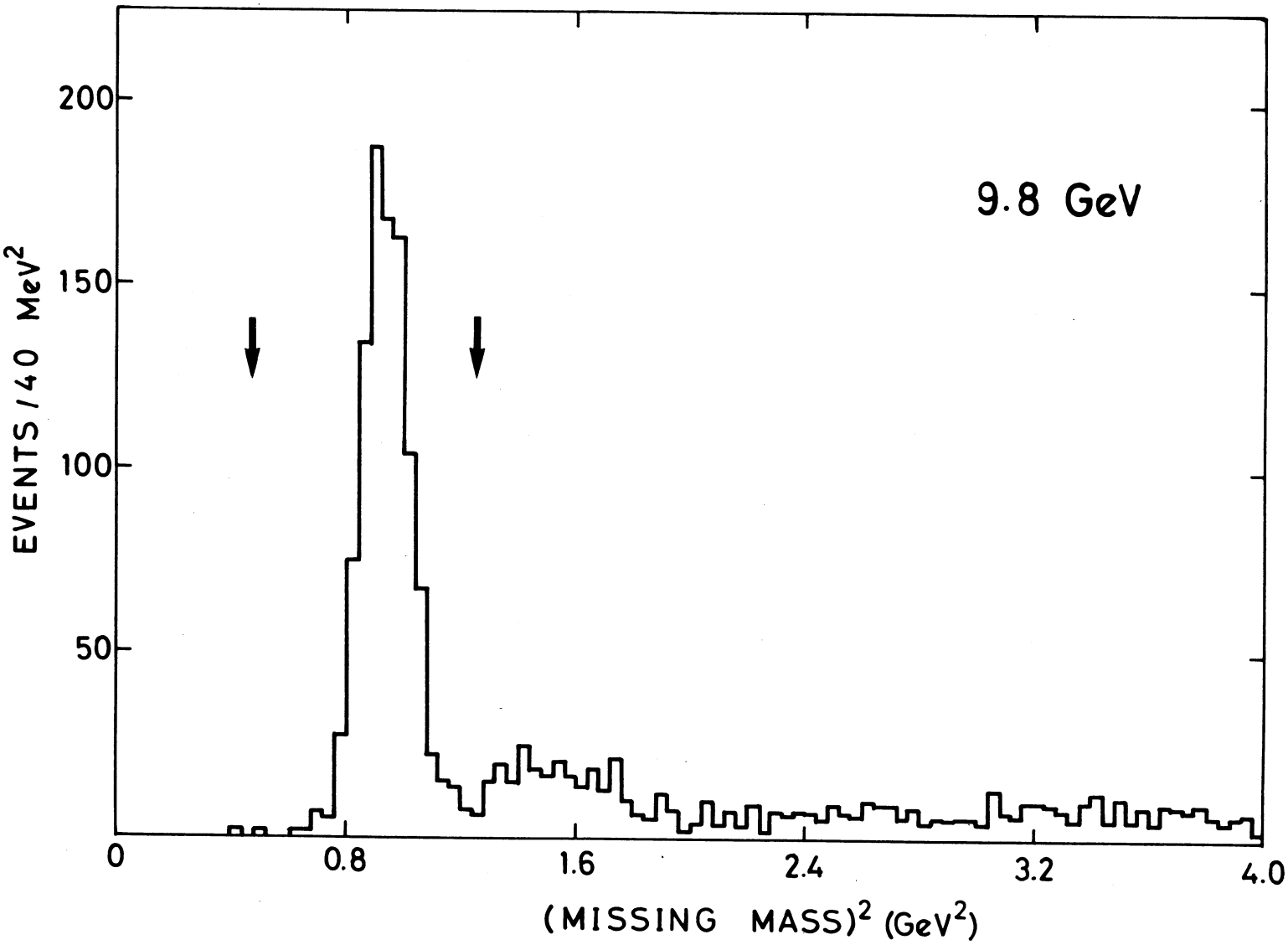
9.8 GeV
EVENTS / 40 MeV²
200
150
100
50
0
0.8
1.6
2.4
3.2
4.0
(MISSING MASS)² (GeV²)

Fig. 3a

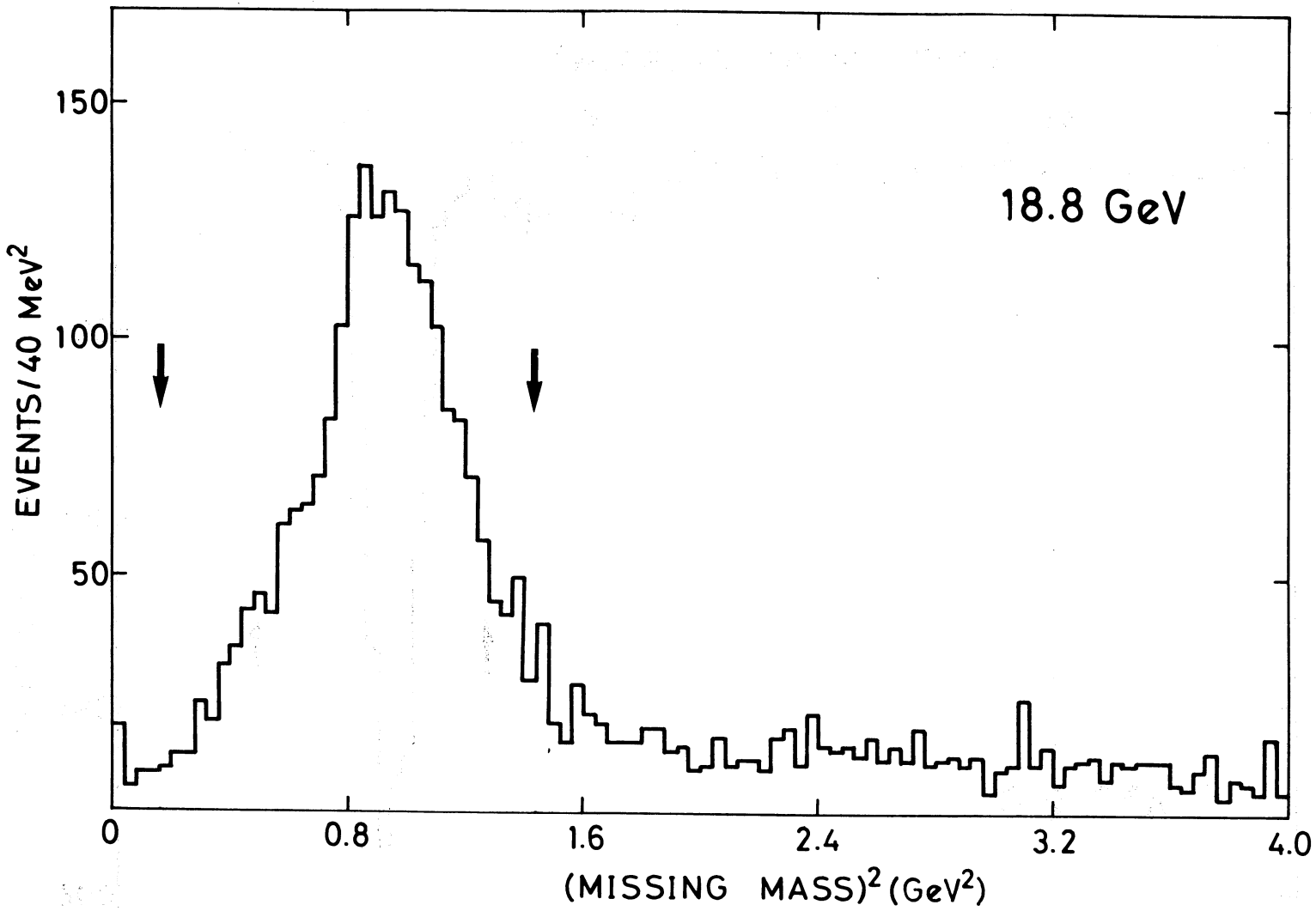
18.8 GeV
EVENTS/40 MeV²
150
100
50
0
0.8
1.6
2.4
3.2
4.0
(MISSING MASS)² (GeV²)

Fig. 3b

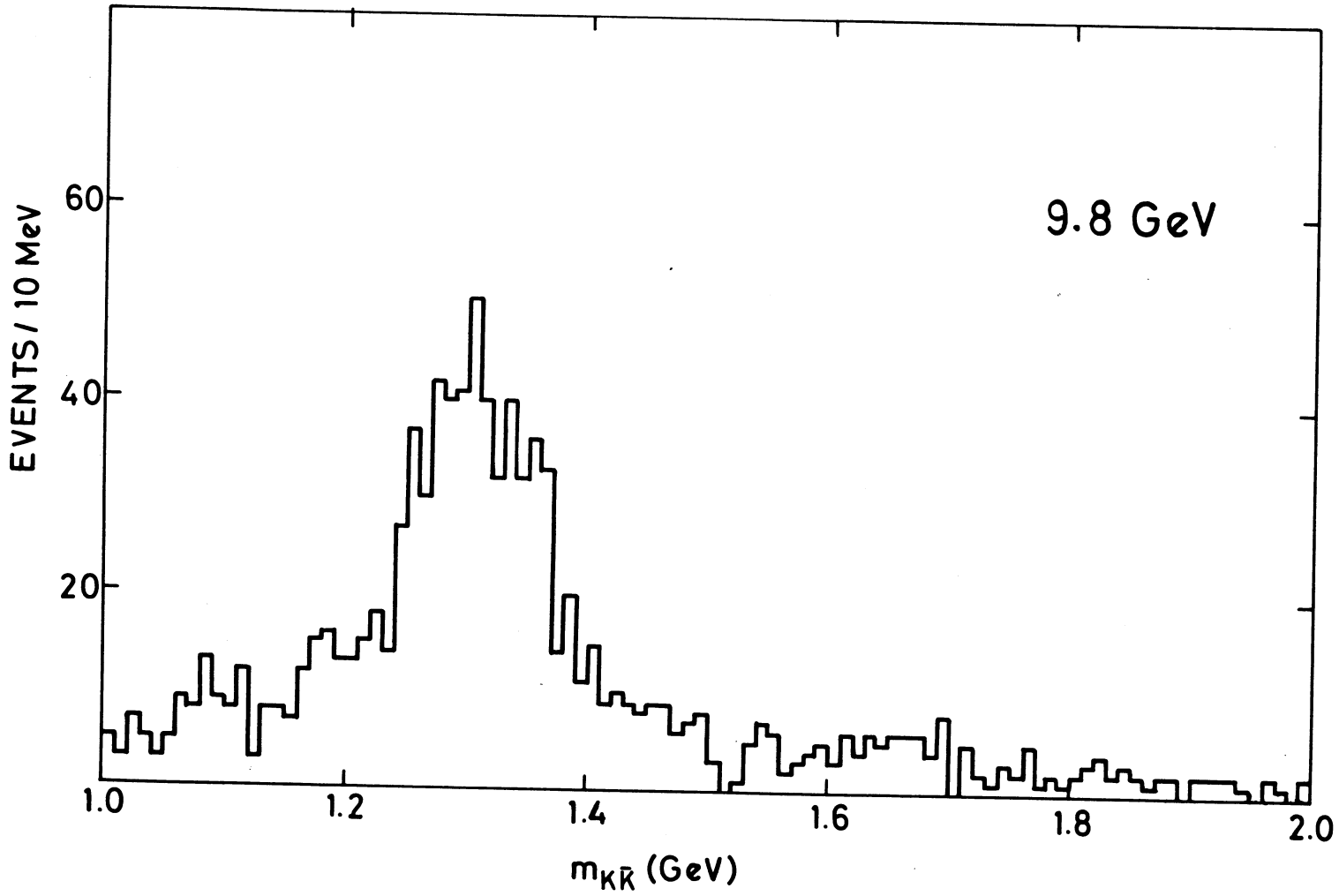

Fig. 4a

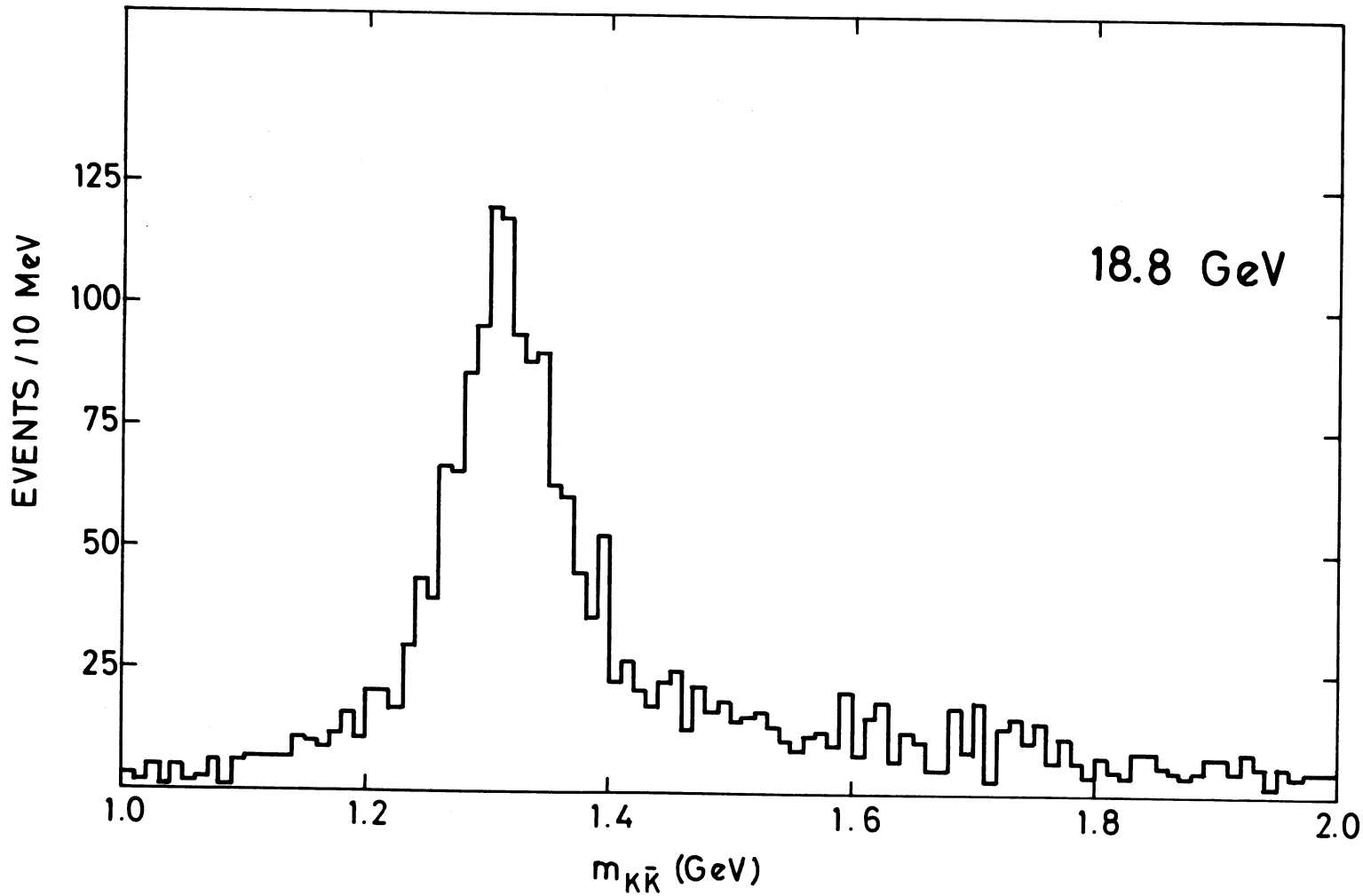
EVENTS / 10 MeV
125
100
75
50
25
18.8 GeV
1.0
1.2
1.4
1.6
1.8
2.0
$m_{K\bar{K}}$ (GeV)

Fig. 4b

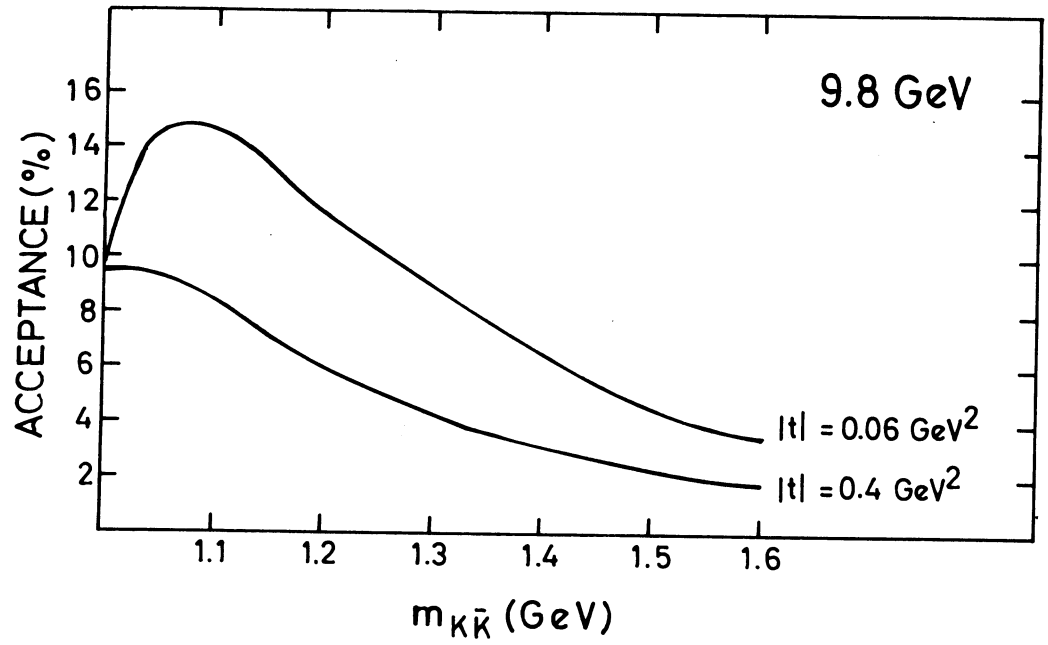
9.8 GeV
ACCEPTANCE (%)
16
14
12
10
8
6
4
2
1.1
1.2
1.3
1.4
1.5
1.6
|t| = 0.06 GeV²
|t| = 0.4 GeV²
m KK̄ (GeV)

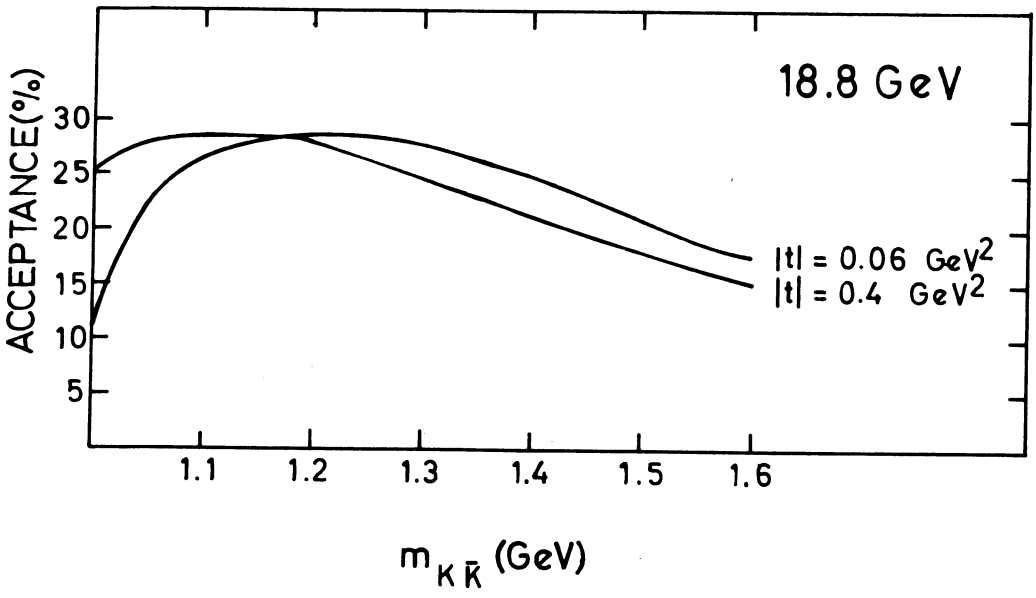
18.8 GeV
ACCEPTANCE(%)
30
25
20
15
10
5
1.1
1.2
1.3
1.4
1.5
1.6
|t| = 0.06 GeV²
|t| = 0.4 GeV²
m KK̄ (GeV)

Fig. 5

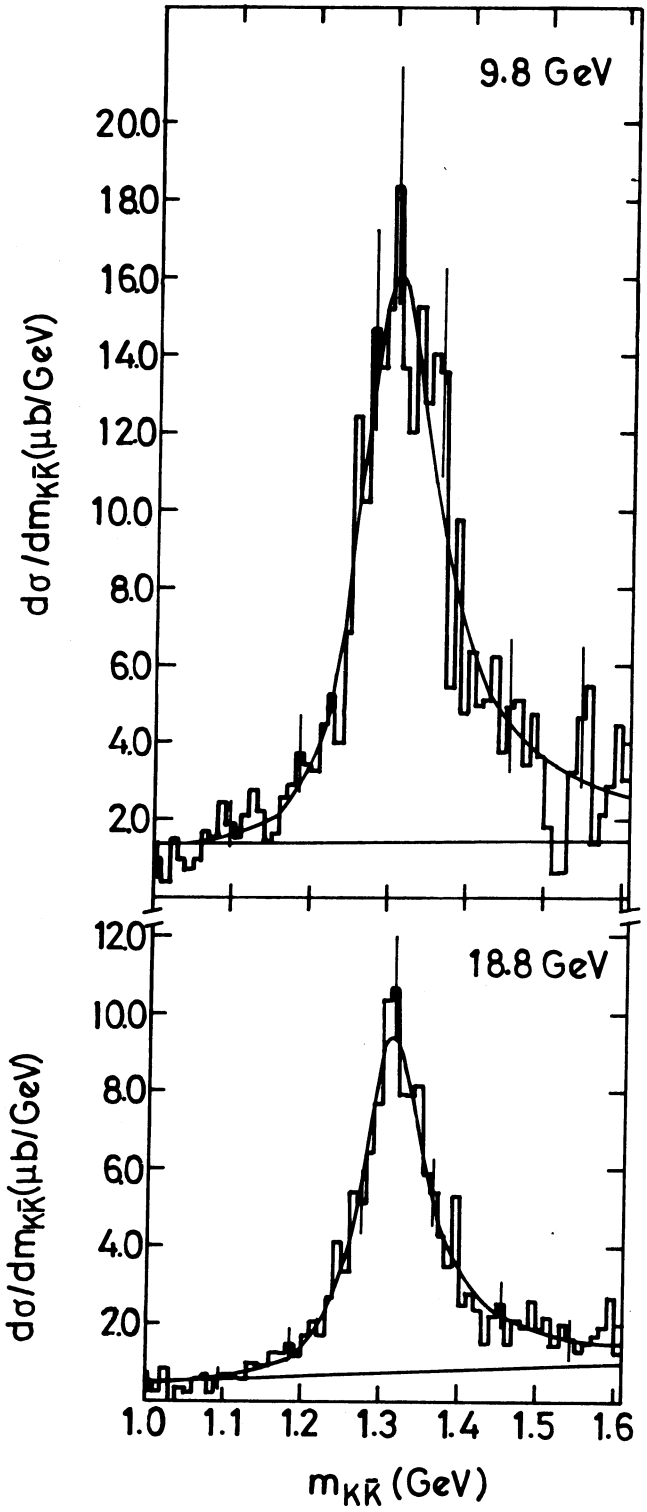
9.8 GeV
18.8 GeV
dσ/dm_KK̄(μb/GeV)
m_KK̄ (GeV)
20.0
18.0
16.0
14.0
12.0
10.0
8.0
6.0
4.0
2.0
1.0
1.1
1.2
1.3
1.4
1.5
1.6

Fig. 6

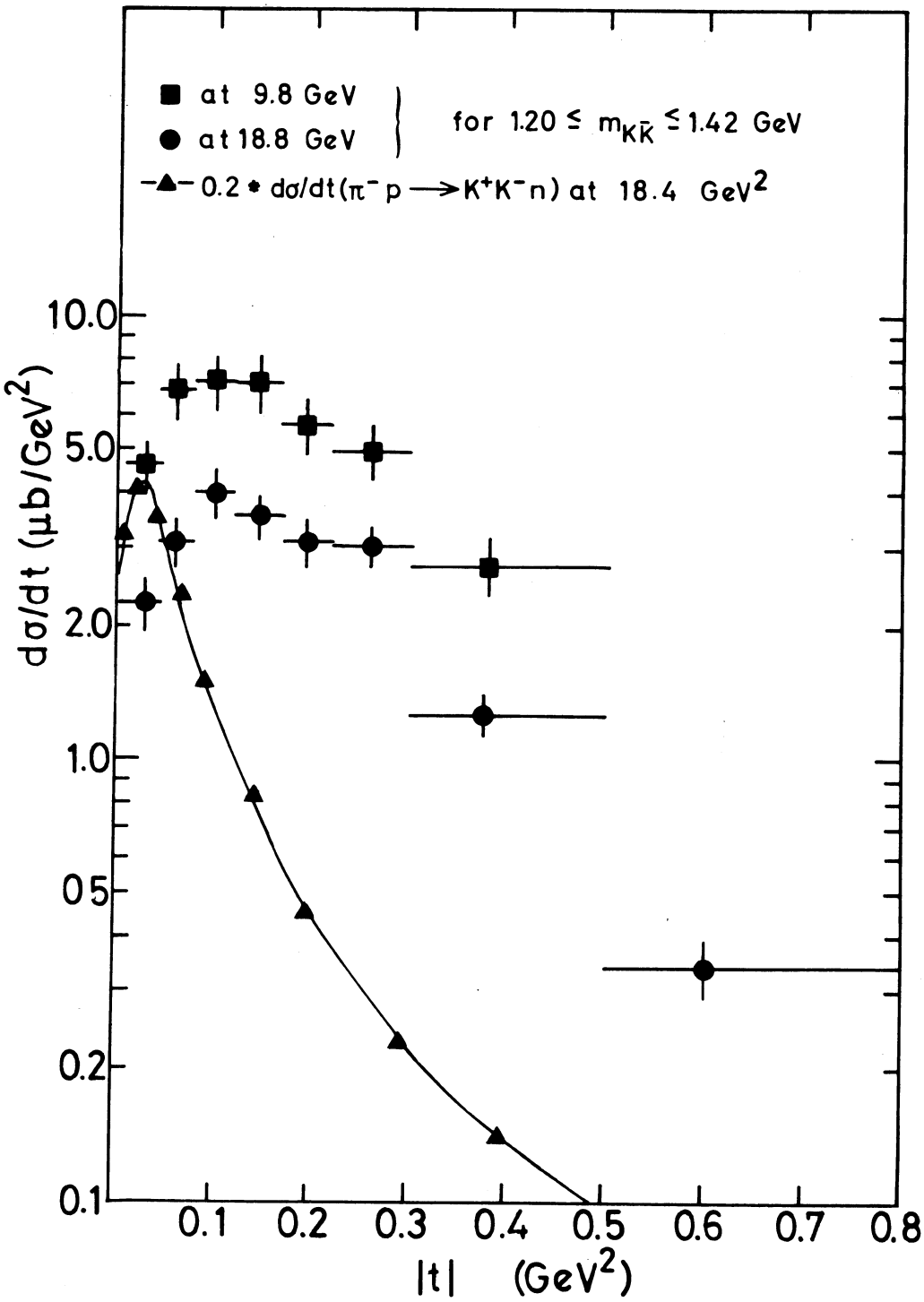
■ at 9.8 GeV
● at 18.8 GeV
for 1.20 ≤ $m_{K\bar{K}}$ ≤ 1.42 GeV
–▲– 0.2 * dσ/dt(π⁻p → K⁺K⁻n) at 18.4 GeV²
dσ/dt (μb/GeV²)
10.0
5.0
2.0
1.0
0.5
0.2
0.1
0.1
0.2
0.3
0.4
0.5
0.6
0.7
0.8
|t| (GeV²)

Fig. 7

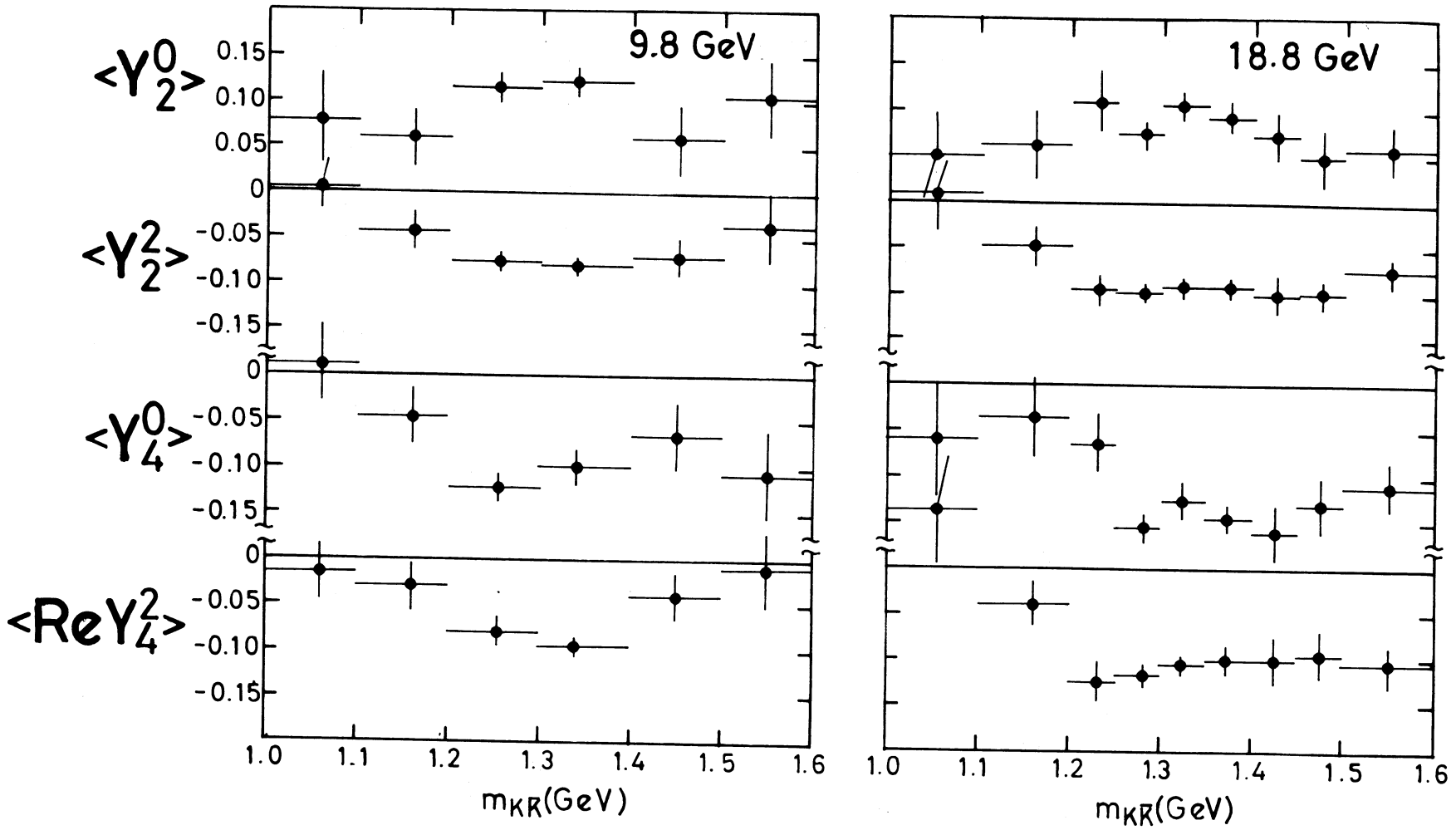
9.8 GeV
18.8 GeV
$\langle Y_2^0 \rangle$
$\langle Y_2^2 \rangle$
$\langle Y_4^0 \rangle$
$\langle \mathrm{Re} Y_4^2 \rangle$
0.15
0.10
0.05
0
-0.05
-0.10
-0.15
1.0
1.1
1.2
1.3
1.4
1.5
1.6
m_{KR}(GeV)

Fig. 8

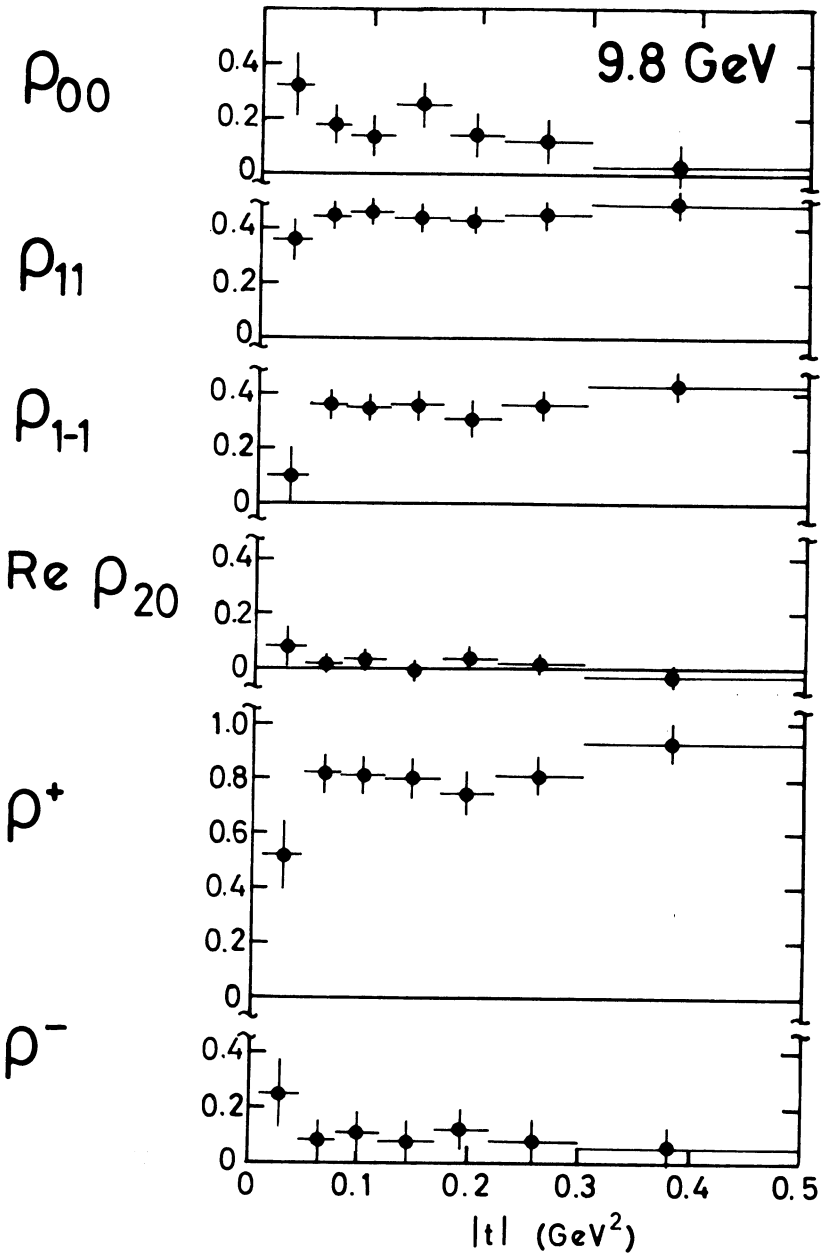
ρ_{00}
ρ_{11}
ρ_{1-1}
Re ρ_{20}
ρ^+
ρ^-
9.8 GeV
0.4
0.2
0
1.0
0.8
0.6
0.4
0.2
0
0
0.1
0.2
0.3
0.4
0.5
|t| (GeV^2)

Fig. 9a

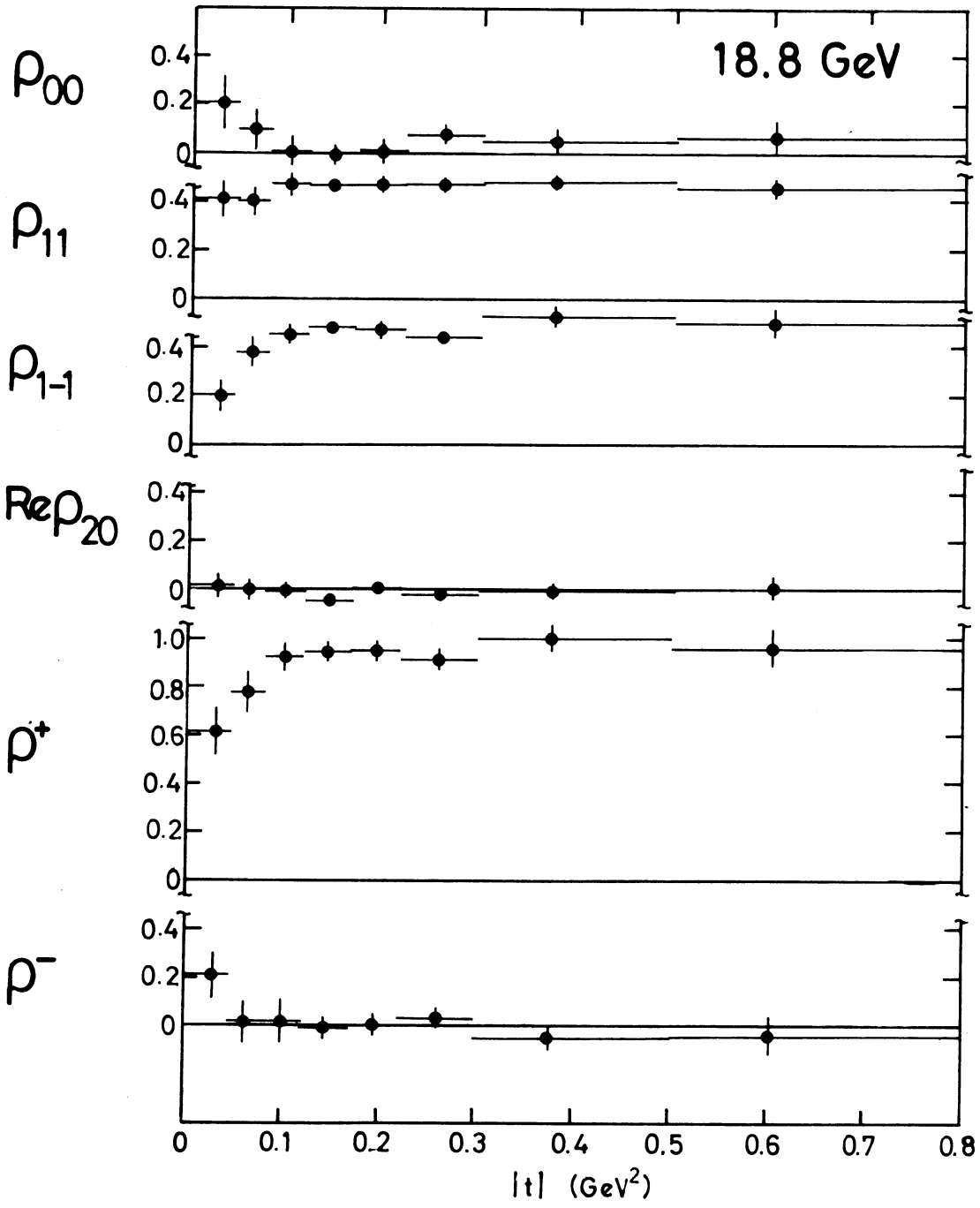
18.8 GeV
ρ_{00}
ρ_{11}
ρ_{1-1}
$Re\rho_{20}$
ρ^+
ρ^-
0.4
0.2
0
1.0
0.8
0.6
0.1
0.3
0.5
0.7
0.8
|t| (GeV^2)

Fig. 9b

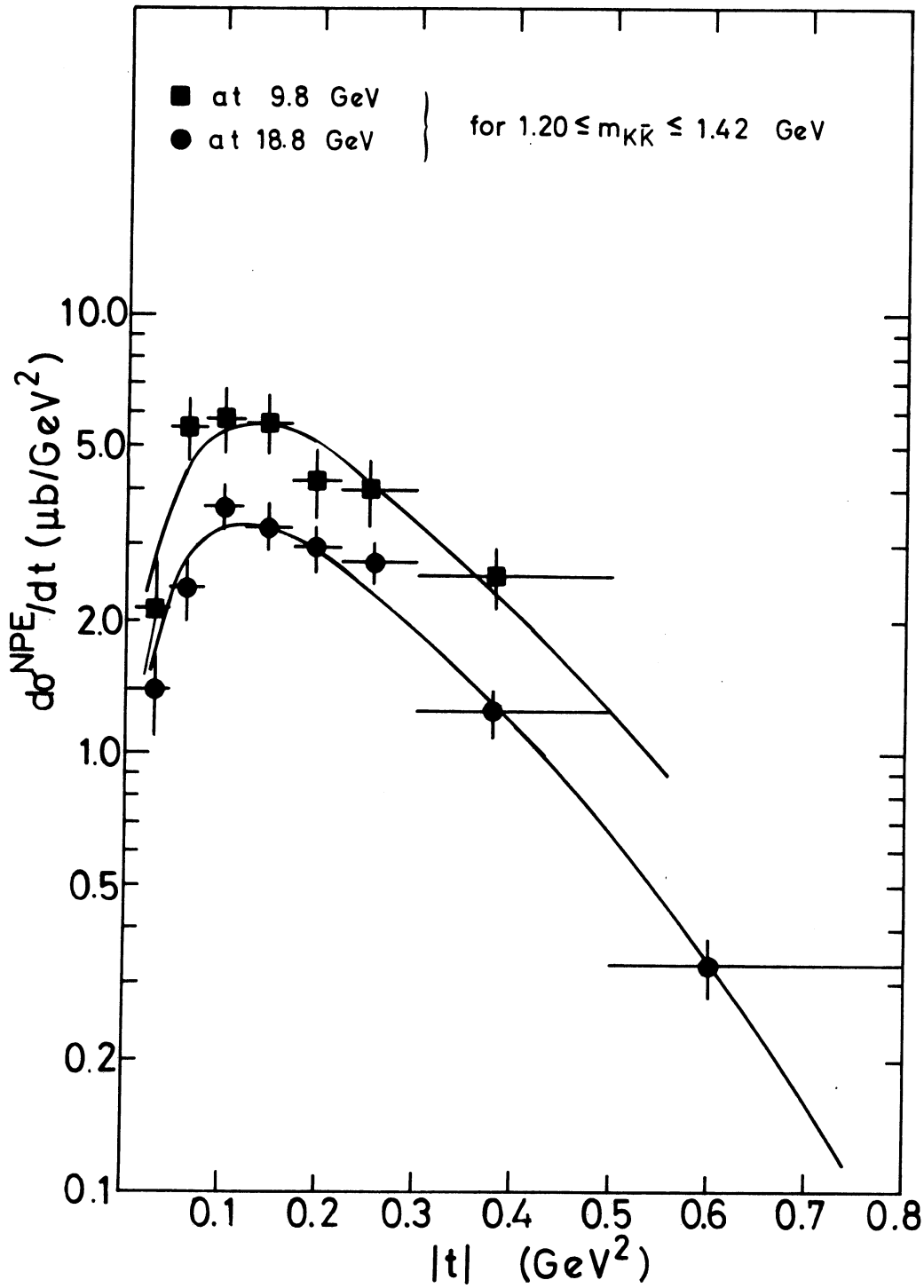
■ at 9.8 GeV
● at 18.8 GeV
for 1.20 ≤ $m_{K\bar{K}}$ ≤ 1.42 GeV
$d\sigma^{NPE}/dt$ (μb/GeV^2)
10.0
5.0
2.0
1.0
0.5
0.2
0.1
0.1
0.2
0.3
0.4
0.5
0.6
0.7
0.8
|t| (GeV^2)

Fig. 10

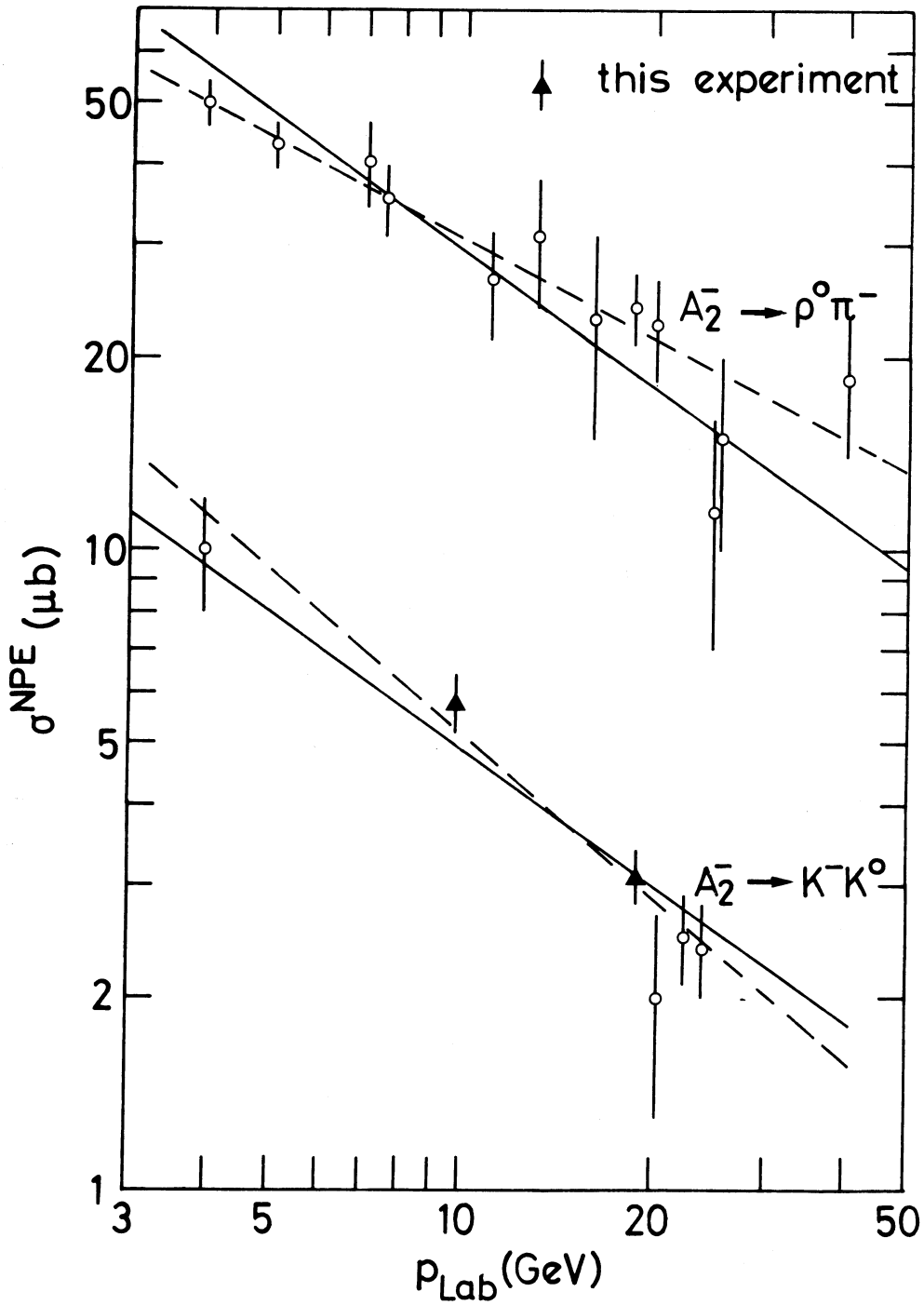
this experiment
$A_2^- \to \rho^0\pi^-$
$A_2^- \to K^-K^0$
σ^{NPE} (μb)
p_{Lab}(GeV)
50
20
10
5
2
1
3
5
10
20
50

Fig. 11